Fermi National Accelerator Lab

Abort Gap Monitoring Utilizing Synchrotron Light

a.k.a. AGI

Randy Thurman-Keup

AD / Instrumentation Deptartment

February 19, 2008

BEAMS-DOC-1390-V3

Abstract

This paper discusses the implementation of abort gap monitoring at the Tevatron. The current system utilizes a fast gateable microchannel plate type photomultiplier tube from Hamamatsu, model number R5916U-50 (but with 3 stages of microchannel plates). There is one connected to each of the proton and pbar Synclite systems. The system can detect as few as 10^7 particles in the DC beam.

1 Introduction

During operation of the Tevatron in colliding beam mode, a small amount of the beam diffuses out of the bunches and spreads around the ring. The presence of beam in the abort gap can have a serious effect on superconducting magnets and a devastating effect on the silicon detector of CDF. During an abort, the kicker magnets ramp up during the abort gap. Beam passing through the kickers while they are ramping sprays into magnets and into the silicon detector. Until the implementation of the abort gap monitor, the only measure of the amount of beam in the abort gap was the count rate in a set of photomultipliers surrounding the beamline at CDF [1] that were gated on the abort gap. The measurements from these counters suffer from the fact that they are measuring the beam leaving the abort gap, not the beam still in it. This document describes an approach to measuring the beam in the abort gap using synchrotron radiation. The radiation, which is normally used by the Synclite emittance measuring device, traverses a beamsplitter where half of it is detected by a microchannel plate (MCP) type photomultiplier tube (PMT).

2 Theory

A charged particle that undergoes transverse acceleration emits radiation in a cone around its velocity vector. This radiation is called synchrotron radiation after its first observation in a synchrotron. See [9], [10], [11], and [12] for the theoretical background and early proton measurements of synchrotron light. Details of the Synclite system are located in [2]. The Tevatron has 1113 RF buckets and typically contains 10^{13} protons in 36 bunches arranged in 3 trains of 12 (the antiproton intensity is ~1/10 the proton intensity).

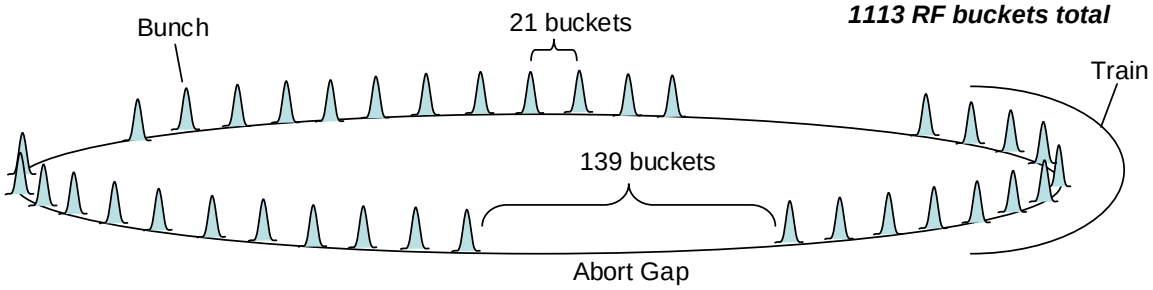

The detection bandwidth for the system is limited on the short wavelength side (400 nm) by the glass of the lens and on the long wavelength side (800 nm) by the photocathode of the PMT. Table 1 enumerates the various expected signals culminating with the expected number of photoelectrons for each particle species per 10^9 particles.

Table 1: List of expected signals and efficiencies for various elements in the system broken up into four wavelength regions. The expected number of photons is taken from a simulation done for the Synclite system [2].

	Protons				Antiprotons			
Wavelength (nm)	**450**	**550**	**650**	**750**	**450**	**550**	**650**	**750**
# of photons / 100 nm / 10^9 particles	15,000	24,000	30,000	37,000	39,000	58,000	80,000	106,000
Optical Efficiency – Mirrors, etc…	30.0%				30.0%			
Quantum Efficiency	13.0%	8.5%	5.5%	2.0%	13.0%	8.5%	5.5%	2.0%
Duty Cycle (1 abort gap)	0.1				0.1			
# photoelectrons	191				496			

3 Apparatus

Figure 1 is a schematic diagram of the Synclite systems illustrating how the light is collected and split off for the AGI systems. Figure 2 is a couple of photos of the proton and pbar AGI systems.

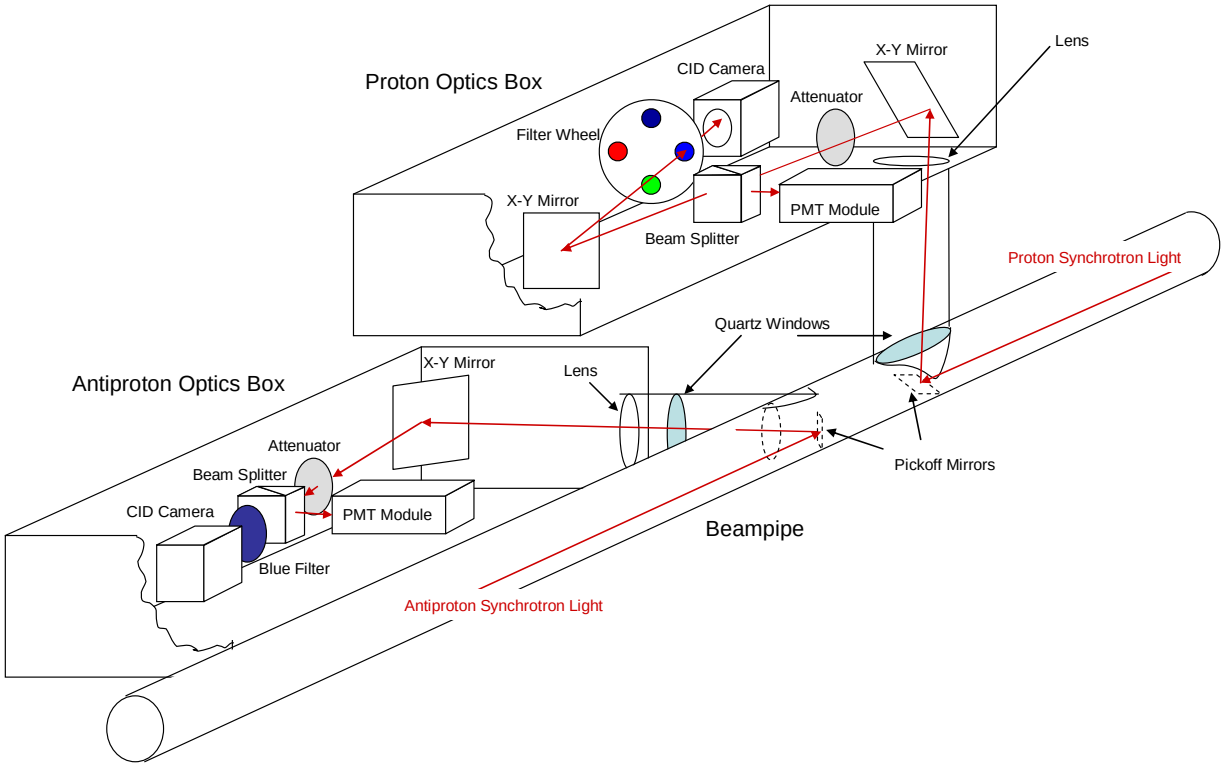

Figure 1: Diagram of Synclite system. The optics through the beam splitter are shared by the Synclite and AGI systems. In addition to the Synclite attenuators, there is a 100:1 neutral density filter in each PMT module. The neutral density filter transmittance is only valid over the visible region [8]. Since the PMT has a bandwidth that extends into the infrared, the effective transmittance of the Synclite attenuators is 21:1 and 6:1 for the proton and pbar systems, and the transmittance of the PMT module attenuators is 55:1 and 44:1 for the proton and pbar PMTs.

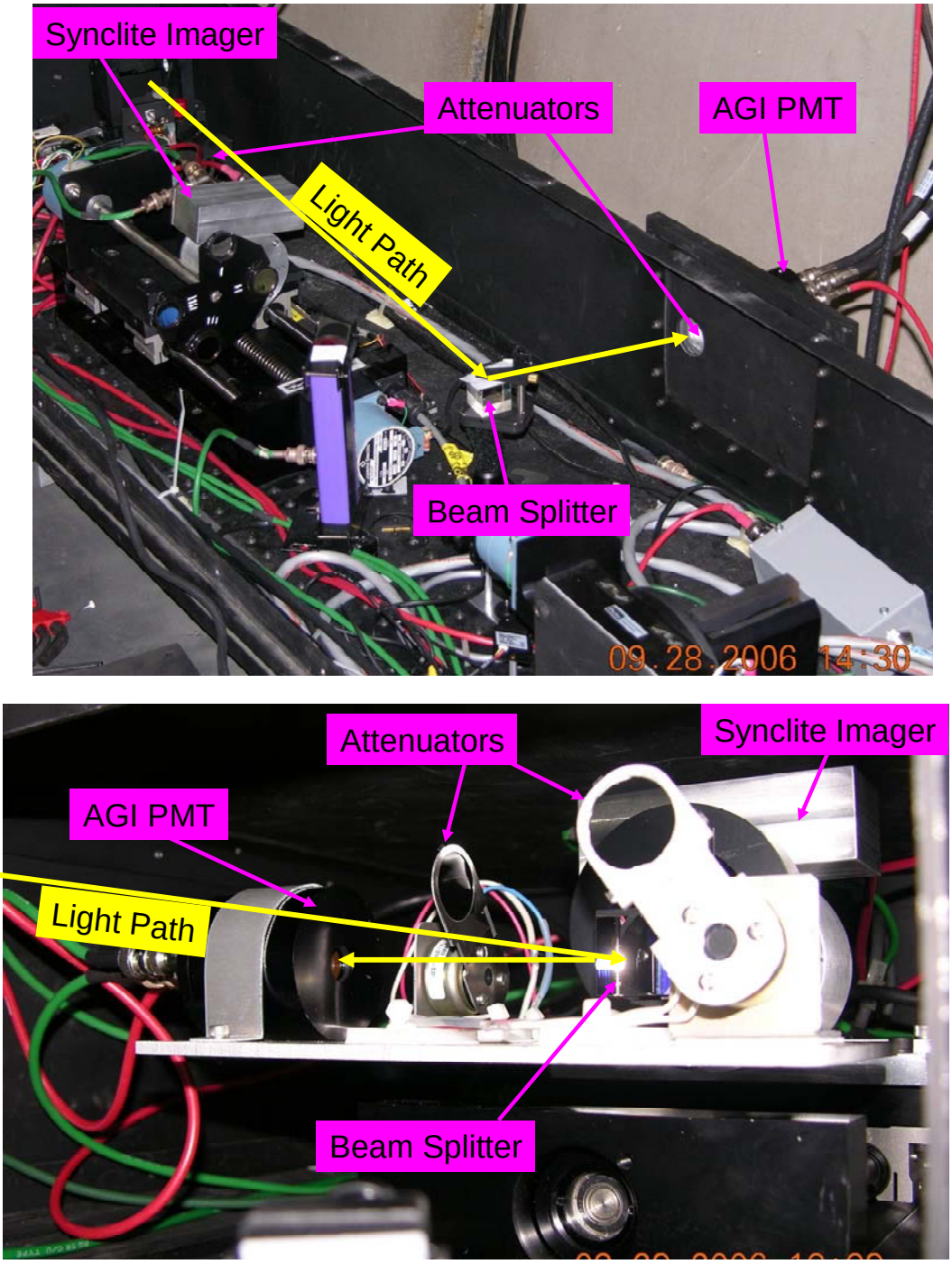

Figure 2: Photos showing details of AGI systems. Top: Proton Synclite box with AGI related devices labeled. Bottom: Inside the pbar box, with AGI devices labeled. The light path in the pbar photo originates in the direction of the camera that took this picture.

The light is picked off by a mirror in the beam pipe [4] and directed out a quartz window [5] to the light box. Inside the proton(antiproton) light box, the light traverses a 1500(750) mm focal length lens [6] and another mirror before hitting the beam splitter 0. The synchrotron light is clearly visible on the wall of the proton light box in Figure 3.

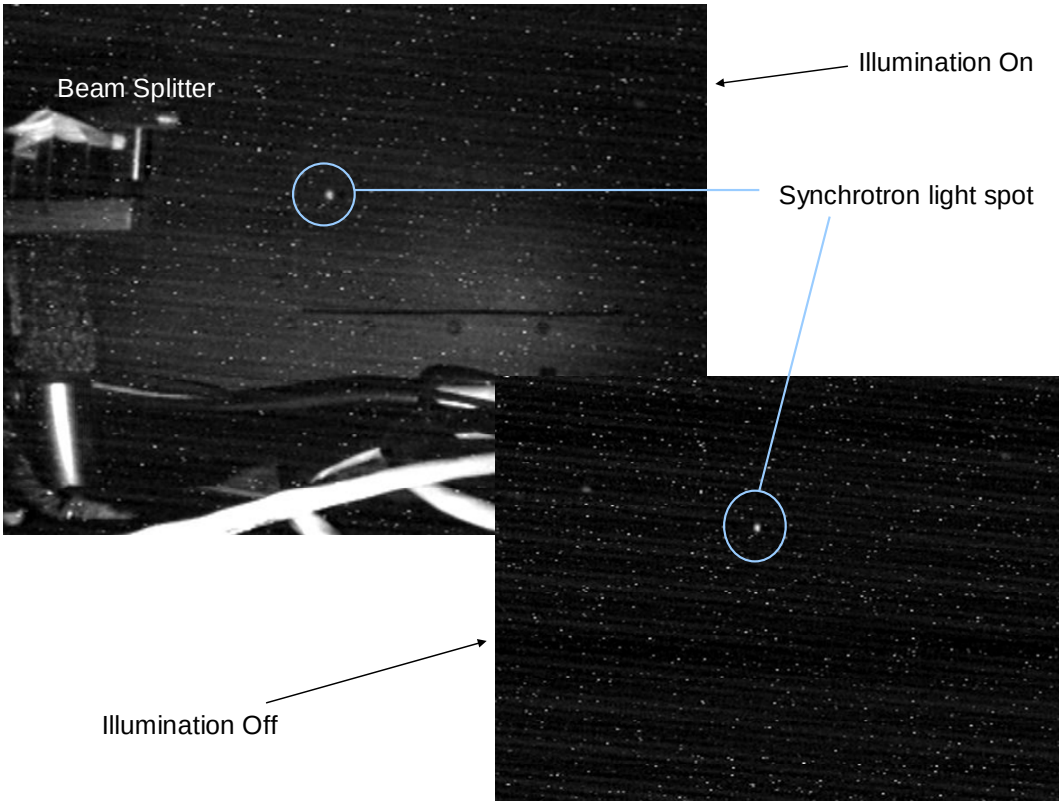

Figure 3: Video stills from a CCD camera mounted in the light tight box showing synchrotron light impacting the side of the light tight box. The smaller white specs are radiation damaged pixels. This image was taken prior to installing the PMT.

After the beam splitter, the PMT and Synclite systems follow separate paths. There are two optical attenuators in each system that can be inserted into the optical path to enable calibration of the PMT. In the proton box, the total attenuation is 1/1155 and in the pbar box, the total attenuation is 1/264. These numbers are measured with the PMT with the filters in and out; so there is an assumption of linearity of the PMT that feeds into those numbers.

4 Synclite Measurement

Prior to the PMT system being installed, an attempt was made to measure the abort gap beam using the Synclite system [2]. The Synclite system functions by using a gated image intensifier to act as a fast shutter and amplifier for a generic CID camera. This allows for the accumulation of many short-duration 'frames' during one 1/30 sec camera frame. The intensifier is operated at a gain of ~1000. The number of times the shutter is opened during a single camera frame is adjusted by the DAQ system based on the measured intensity. In the case of the abort gap, this is typically every 2^{nd} turn (~25 kHz). A LabVIEW DAQ system [13] collects the camera frames and fits horizontal and vertical projections of the beam profile to obtain the integrated intensity. Each abort gap measurement is the sum of 200 camera frames, or 8×10^4 abort gaps. Camera data of the abort gap are displayed in Figure 4 and Figure 5. The bump corresponds to a DC beam intensity around the ring of ~5 E9. Presently, the proton Synclite system has a lower limit sensitivity of around 4-5 E9 due to changes in the bandwidth of the filter.

Abort Gap Light, TEL Off

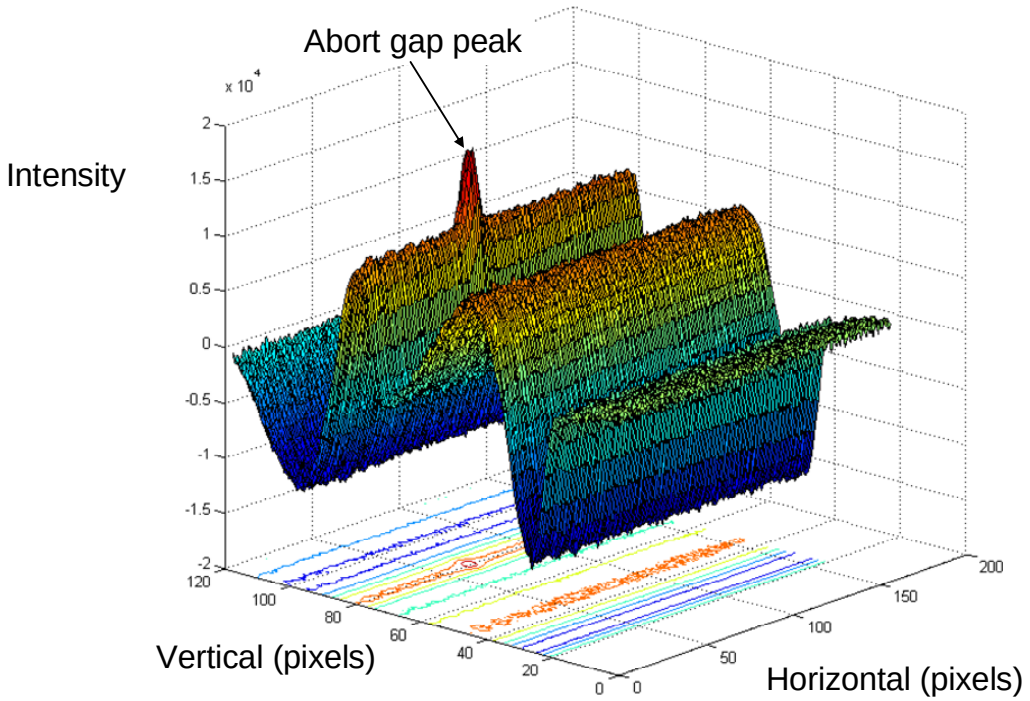

Figure 4: Camera image in abort gap. This is after pixel by pixel background subtraction, but before horizontal line subtraction. The peak corresponds to a DC beam intensity of ~5 x 10^9. The vertical undulations are the typical horizontal bands one sees in an analog video signal caused by noise. Conditions have improved since these plots. See Section 6 for details about background subtraction.

Abort Gap Light, TEL Off, background subtracted

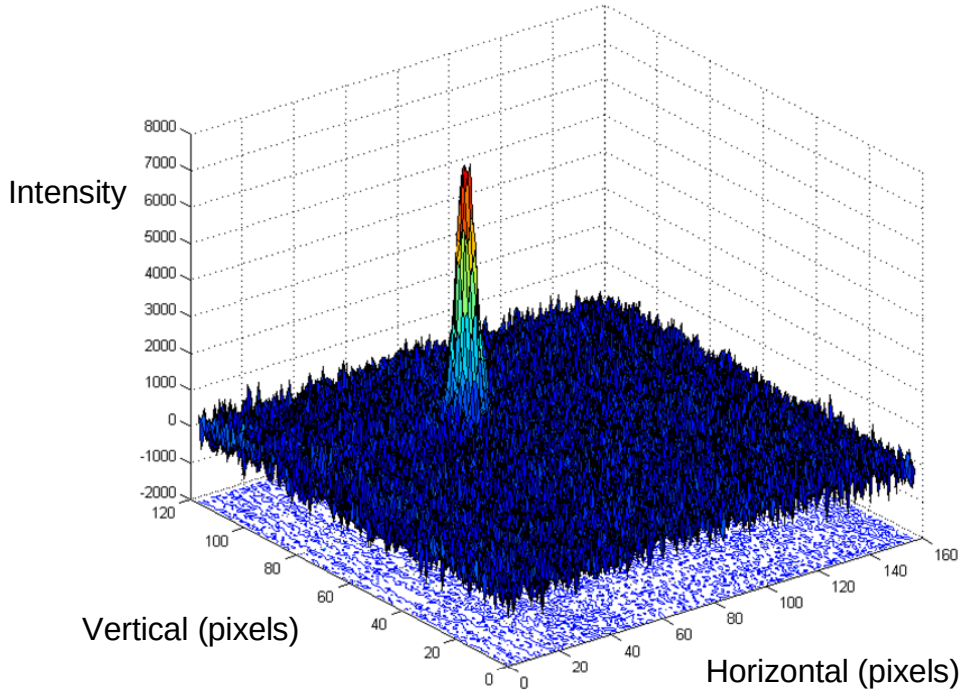

Figure 5: This image is after both pixel and horizontal line subtraction. The peak corresponds to a DC beam intensity of ~5 E9.

5 PMT System

Information about the original dynode-gated PMT can be found in Appendix A.

5.1 Gated PMT

The PMT being used in the AGI system is a modified Hamamatsu R5916U-50 (built with 3 stages of microchannel plates) and has a maximum gain of ~10^7. Its most notable feature is its fast gating capability; it has a minimum gate width of 5ns. It also has a large extinction ratio and no detectable sensitivity to light present before the gate is applied. Figures 6 and 7 show some test results from the PMT. Additional plots are in Appendix C.

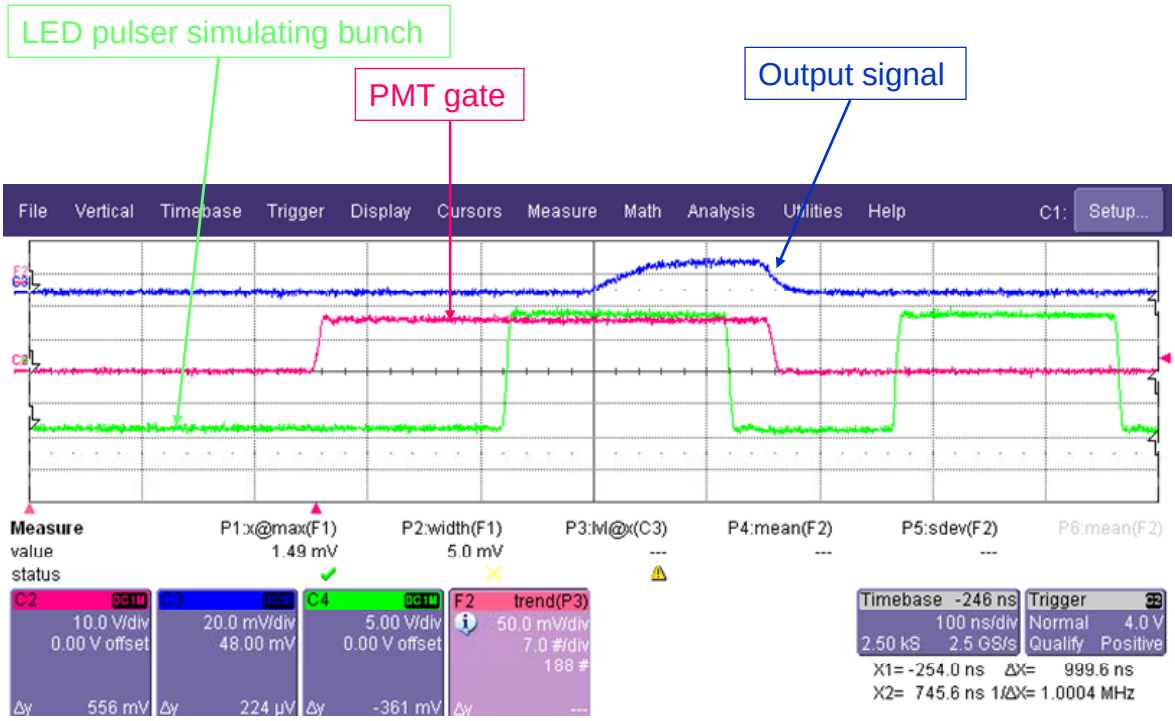

Figure 6: Plot showing the response of the PMT output to an LED pulse while the gate is on. The rising edge of the response is presumably the slow turn on time of the LED which is a function of the series resistor and the capacitance of the LED among other things. The trailing edge of the response is somewhat sharper. The time from end of LED pulse to end of signal decay is at least 80ns on the scope.

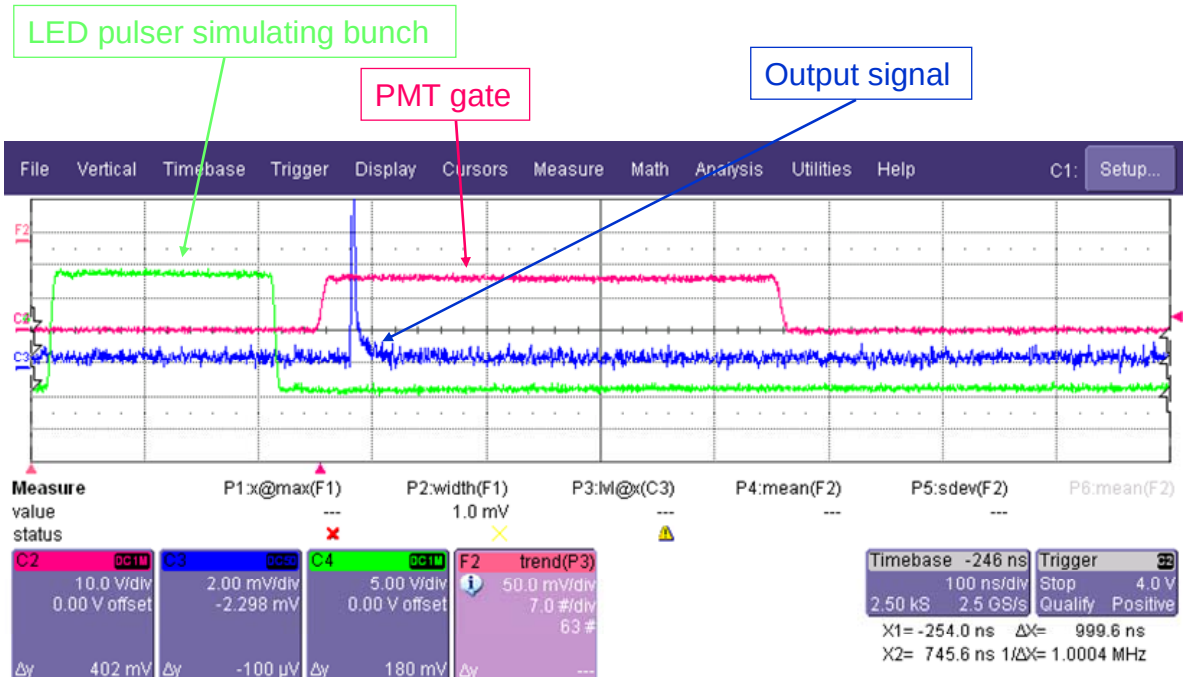

Figure 7: Testing for sensitivity to pre-gate light. The LED gate is slowly moved back until a signal is observed from the PMT. The timing of this observed signal is consistent with the decay of the LED and not something due to the PMT.

5.2 Data Acquisition

5.2.1 Hardware

The DAQ system (Fig. 9) consists of a 5-slot VME crate with an MVME 2434 crate processor running VxWorks that talks to a COMET 12-bit ADC board and a VRFT board for beam timing. Also in the crate is a fast integrator designed by Brian Fellenz. The timing gates for the PMT, integrator, and digitizer, are generated by the VRFT board from $AA markers. The $AA markers are timed in via a NIM delay module. The PMT requires its gates to be greater than 10 Volts, so the timing signals generated by the VRFT are passed through a TTL → 15V amplifier also designed and built by Brian Fellenz. This amplifier, a Droege High Voltage power supply, and the delay module reside in a NIM bin. The present PMT high voltage settings for the proton and pbar systems are 3664 and 3352 volts respectively. The PMT anode signal is brought upstairs to the integrator which feeds the ADC board, and the ADC board is read out by the DAQ program running on the crate processor. The DAQ cycle is triggered by Synclite between its readout cycles, since when Synclite is pulsing, there is noise in the AGI system. A measurement cycle in AGI typically happens every 4-5 seconds and lasts for about 500 ms. For explicit details about the connections between the various components, see Reference [3].

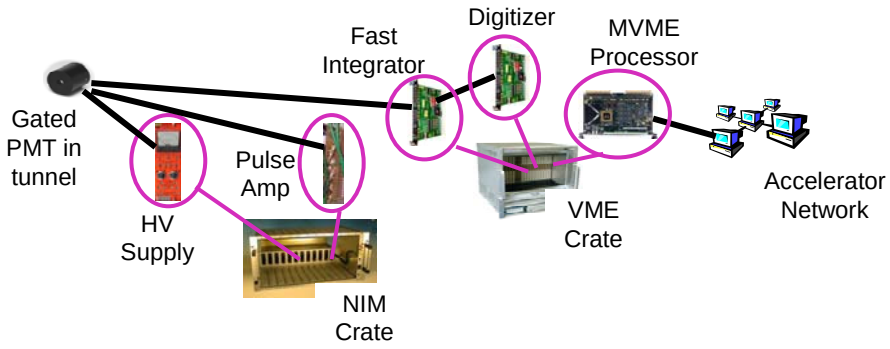

Figure 8: System interconnections. Not shown here is the VRFT board and the $AA marker delay module.

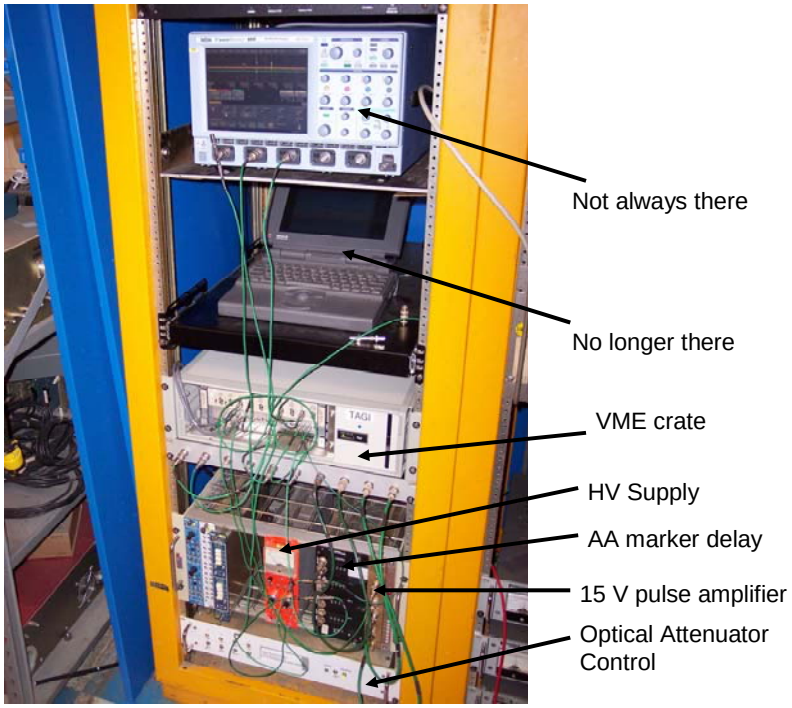

Figure 9: AGI Hardware in the C0 Service Building in rack RR C001. The Apple laptop is no longer part of the system. Instead the Debug connection on the VME Crate Processor is connected to the Synclite PC com port.

5.2.2 Software

The DAQ process consists of two distinct measurements: the abort gaps, and a map of 1/3 of the ring with single bucket sampling known as the DC beam measurement. There are three files read by the AGI when it starts up: a settings file (ppbarsettings.dat), a backgrounds file (ppbarbackgrounds.dat), and the map of how to do the DC beam gating (dcbeam.dat). All three of these are kept in the /fecode-bd/vxworks_write/fe/tagi/ directory on nova.fnal.gov. Figure 10 illustrates the timing details of a measurement cycle. Each measurement cycle consists presently of 1000 'readout cycles' with each readout cycle containing the proper gating for one digitization of each quantity being measured. In practice, the 1000 readout cycles are

accomplished by having the VRFT board replay a single readout cycle 1000 times. When triggered by Synclite, the AGI performs one proton measurement cycle and one pbar measurement cycle. Within each readout cycle, there are pedestal measurements taken at the same relative timing as the data measurements. These pedestal measurements are meant to track the changes in the baseline due to temperature fluctuations of the integrator, EMF changes in the tunnel, etc…

The front-end code for the AGI is kept in the CVS repository on nova.fnal.gov in the TAGI project. There is a README file as part of the repository that explains the contents of the TAGI repository and contains a brief history of changes to the program.

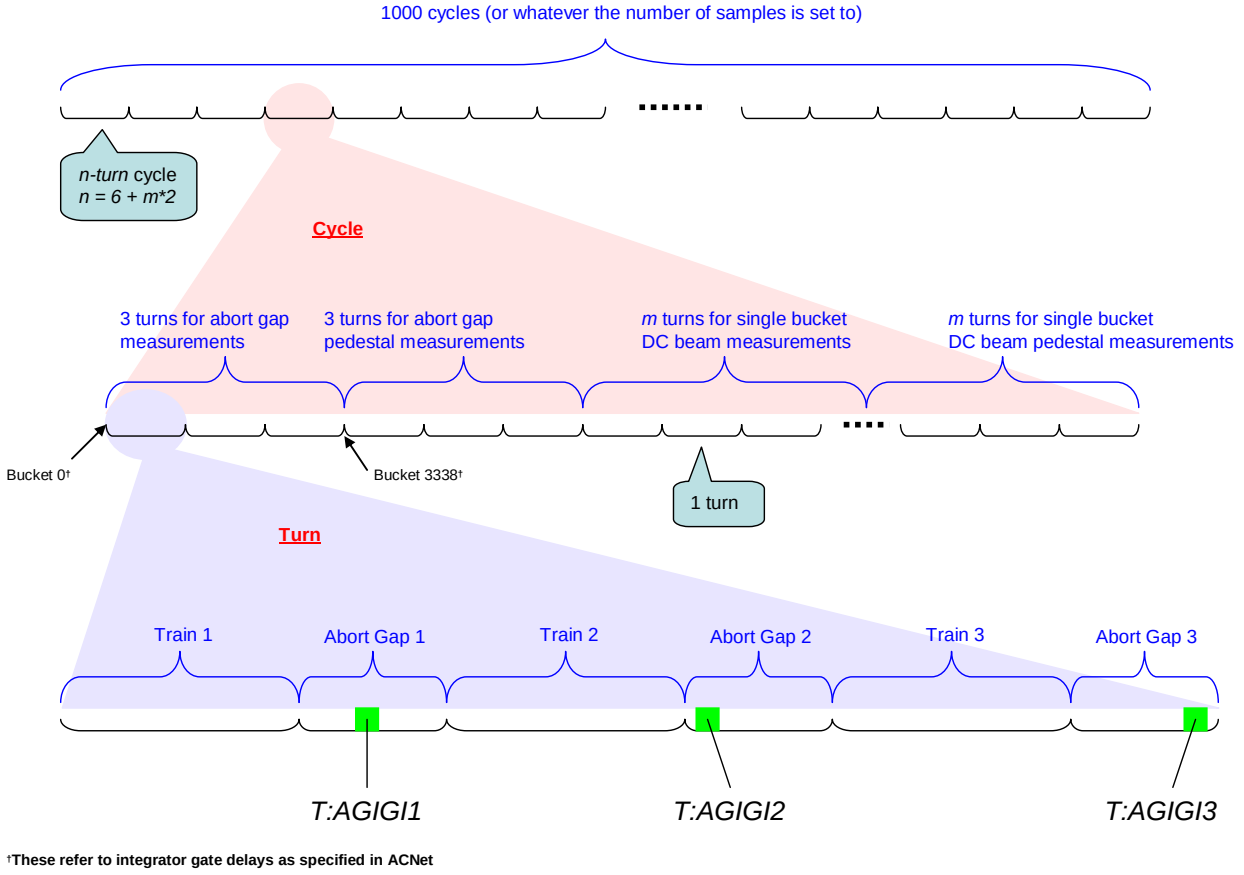

Figure 10: Diagram of DAQ timing. There are 1000 (or whatever the parameter is set to) cycles each with *n* turns. *n* is equal to 6 turns plus twice the number required for doing the DC beam measurement. Presently, there are 3 turns used for doing the DC beam measurement (this number is in the dcbeam.dat file). Since there is not enough time in one cycle to sample all the buckets specified in the DC beam measurement, only a portion of them are sampled. Then during the next measurement cycle, the next group of buckets is sampled. Additionally, the samples can't be consecutive buckets. They must be interleaved so that the ADC has time to reset. That is why a file is read that tells the DAQ program which buckets to sample and in what order.

5.3 User Interface

There are two user interfaces: one is a menu driven display that runs through the serial port of the MVME crate processor, and the other is 3 parameter pages in ACNET. The menu interface and

the ACNET pages both allow you to change the parameters of the program. The ACNET parameter pages also have access to neutral density filter operation. The ACNET pages are on T43 – SLIGHT, subpages 26, 27, and 28. Pages 26 and 27 are the proton and pbar values and parameters. Page 28 has system parameters, such as triggers to perform calibrations and background measurements, control of the filters, a reboot switch, and the MADC readings from the HV supplies.

6 Calibrations

6.1 Baseline Measurement

The baseline determination is done manually by inserting the neutral density filters and taking a measurement in the abort gap. It is preferable to do this while beam is in the Tevatron since EMF noise conditions change depending on the state of the accelerator. Figure 11 shows the drift in the baseline with both the previous PMT/algorithm and the new PMT/algorithm. The stability is much better with the new system.

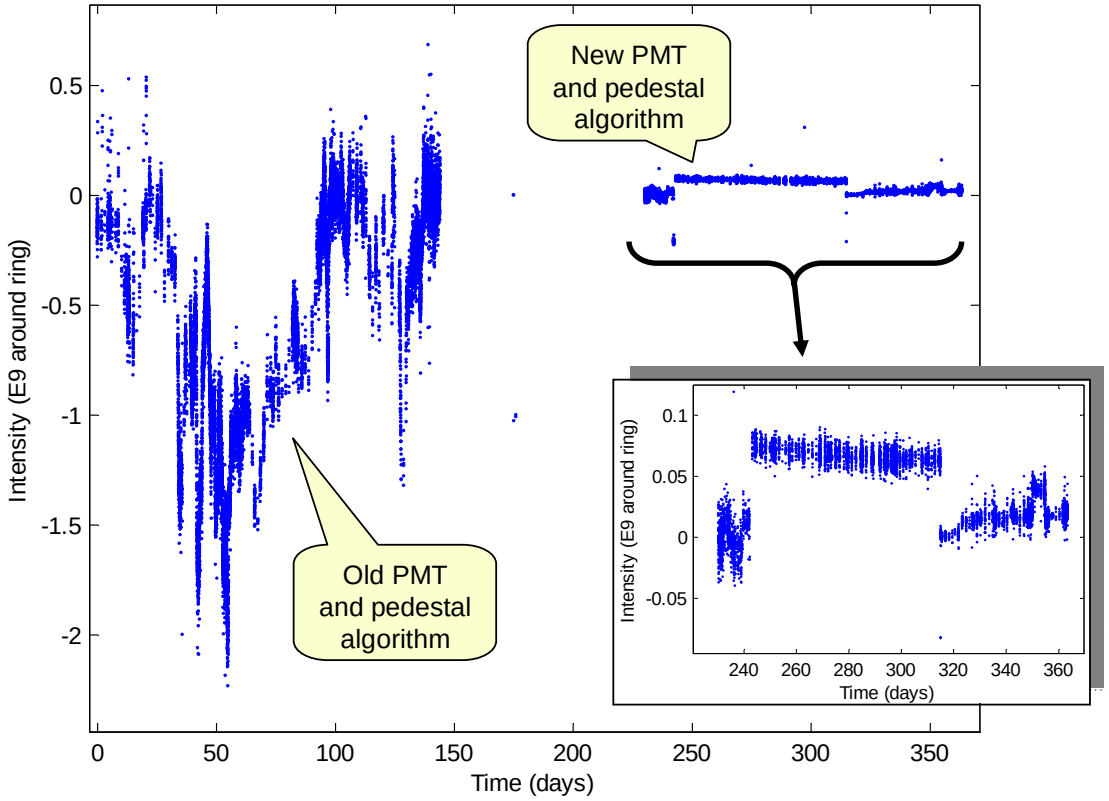

Figure 11: Pedestal drift over the past year including both the old PMT and pedestal algorithm, and the new PMT and algorithm. The stability is now better than 0.1 E9 compared to > 1 E9 before.

6.2 Bunch Based Gain Calibration

The gain of the system can be calibrated from a bunch by inserting the neutral density filters and moving the gate such that it coincides with a bunch. There is code in the front end to do the data collection and calculation automatically. The neutral density filters were calibrated by lowering the voltage of the PMT, positioning the gate over a bunch, and taking measurements with and without the filters in place. This of course assumes that the PMT is fairly linear with input

intensity. Using this approach, the filter values were measured to be 55:1 and 21:1 for the proton attenuators, and 44:1 and 6:1 for the pbar attenuators.

6.3 TEL Based Gain Calibration

Studies have been done by turning off the Tevatron Electron Lens (TEL) and observing the increase in the abort gap beam (see Figure 12). The increase measured by the AGI system is compared with the total beam intensity as measured by a DCCT device[1]. The DCCT device measures the total beam intensity with great resolution. The total beam intensity in the ~180 minutes before the TEL was turned off are fit with a quadratic to obtain the baseline intensity shape. This fit is extrapolated under the TEL off region to obtain a measurement of the 'extra' beam present due to the TEL being off. The agreement of the DCCT measurement with the AGI measurement is quite good indicating that the bunch based calibration is accurate.

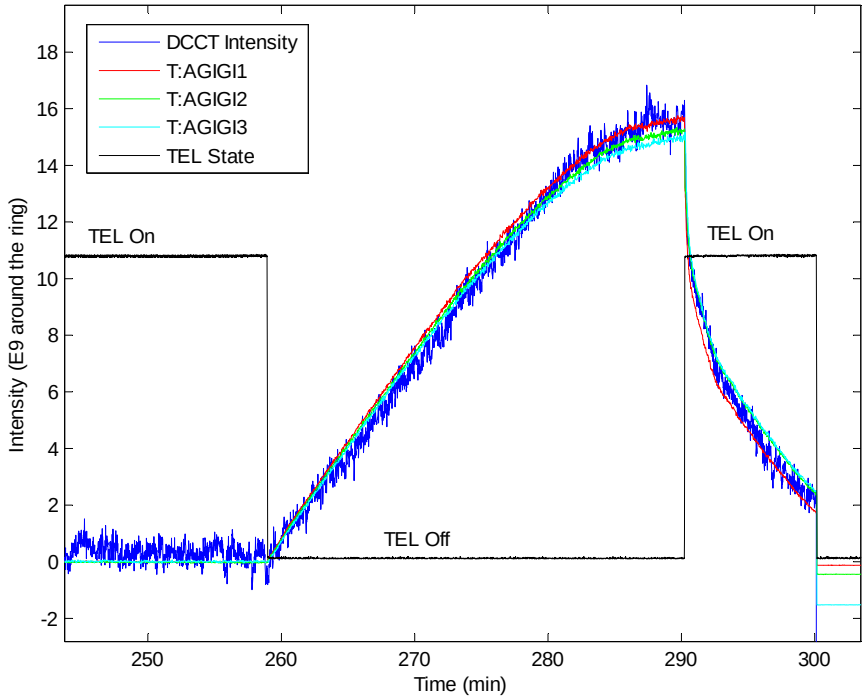

Figure 12: Plot of total beam and beam in the abort gap. These plots have all had baseline subtraction done. The DCCT subtraction is a line rather than a constant since it is a falling spectrum.

One can also look at the pbar abort gap intensity during the TEL study. Figure 13 is a plot of the pbar abort gap intensities during the TEL study. The increase is also observable there, but is about ~10^3 less than the proton gaps.

As an additional check of the calibrations, one can compare the proton and pbar systems given the operating voltages, operating scale factors after calibration, and expected optical luminosities as calculated in the Synclite document. If the calibration is correct, the following should be true.

[1] The amount of beam in the abort gap is inferred from the DCCT (DC current transformer) measurement by comparing the beam loss rate with the TEL on to the beam loss rate with the TEL off and assuming that the decrease in the loss rate is because the DC beam is not being removed by the TEL.

$$\frac{I_P}{I_A}\times\frac{G_P}{G_A}\times\frac{SF_P}{SF_A}=1 \qquad \textbf{(1)}$$

Here *I* is the expected synchrotron radiation intensity, *G* is the gain of the PMT, and *SF* is the scale factor determined by the calibration (P and A indicate proton and antiproton). With the gains obtained from the final test sheet gain vs. voltage plot of the PMTs, and the expected intensity ratio of 1 / 2.7 obtained from the Synclite studies using a numerical calculation, the equation works out to be

$$\frac{1}{2.7}\times\frac{12\times10^5}{8\times10^5}\times\frac{1}{0.6}=0.92\approx1 \qquad \textbf{(2)}$$

which is pretty good agreement.

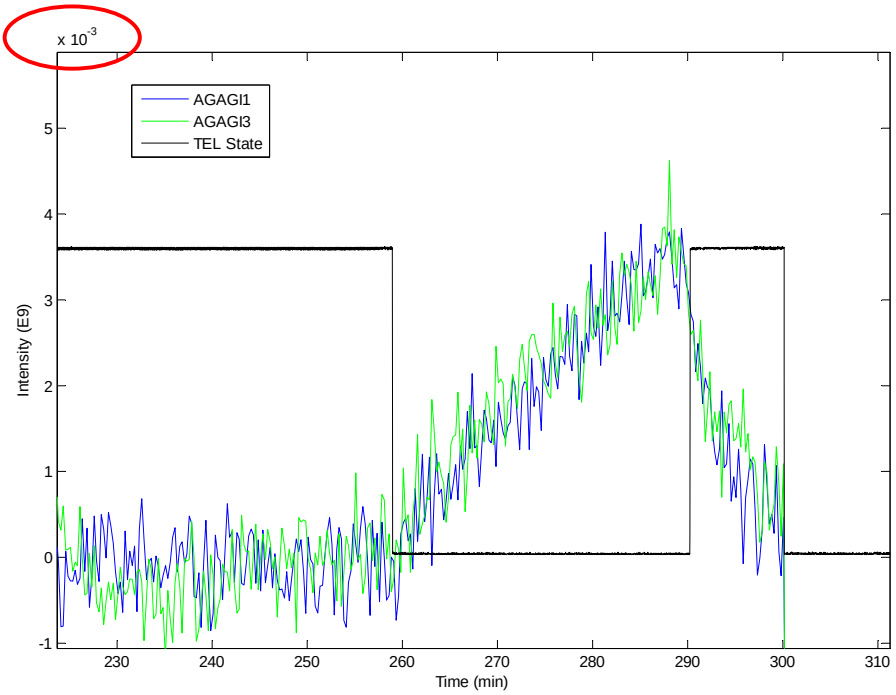

Figure 13: Pbar abort gap levels during the TEL study. The levels are 10^3 less than the proton levels, but they are still visible. From this plot, one can deduce the sensitivity of the pbar monitor. It can detect a DC beam of ~10^6 particles.

7 Summary

The abort gap monitor is functioning extremely well with the new PMT and new algorithms. The stability of the pedestal is better than 0.1 E9 compared to >1 E9 with the previous system. The agreement between bunch calibration and TEL calibration is very good.

8 References

[1] **BEAMS-DOC-976**. Several documents on CDF abort gap counters and such.

[2] **BEAMS-DOC-1975**. Detailed document about the Synclite system, including simulations of synchrotron radiation.

[3] **BEAMS-DOC-1098**. High level hardware schematic of both Synclite and AGI systems.

[4] Aluminized Mirror. Loss is typically 10%.

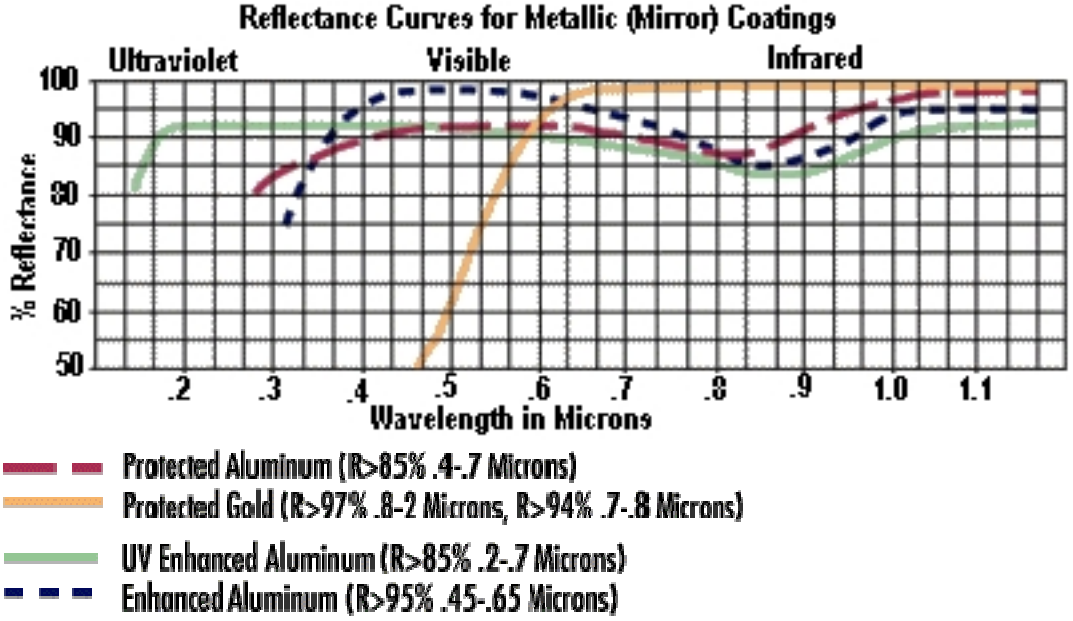

[5] MDC Vacuum Products quartz window #450023 or #450024. The transmission of the quartz window is curve number 2 below (90% for 400-500nm).

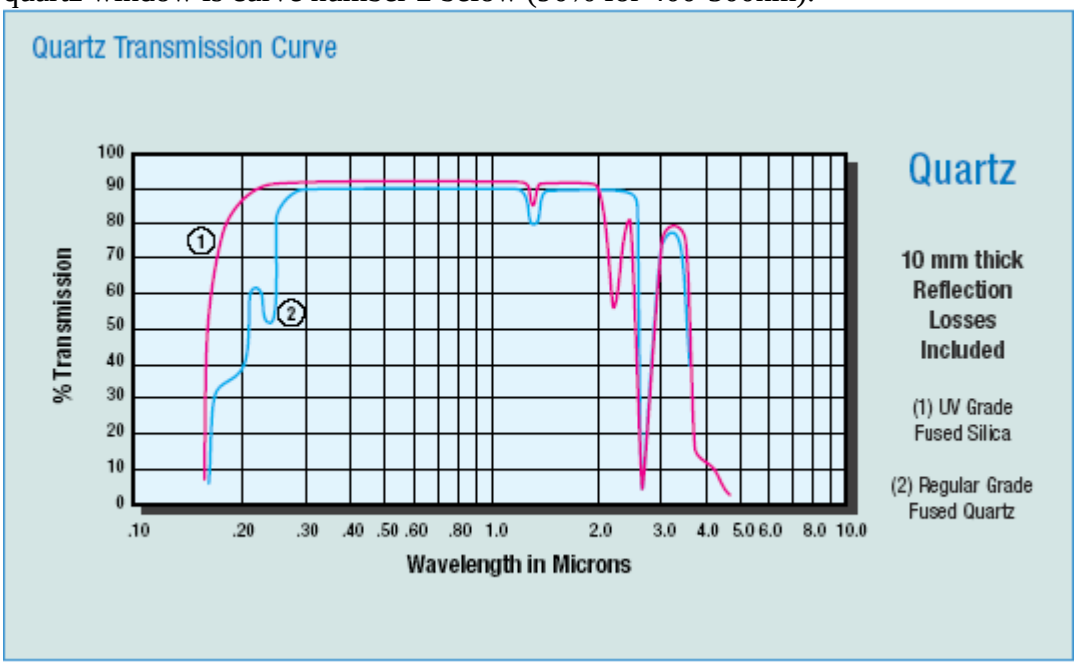

[6] Oriel (now Spectra-Physics) 2” DIA plano convex lens #40825 made of BK 7 glass with 1500 mm focal length and 1495.6 mm back focal length. Transmittance for BK7 glass is shown below (93% for 400-500nm).

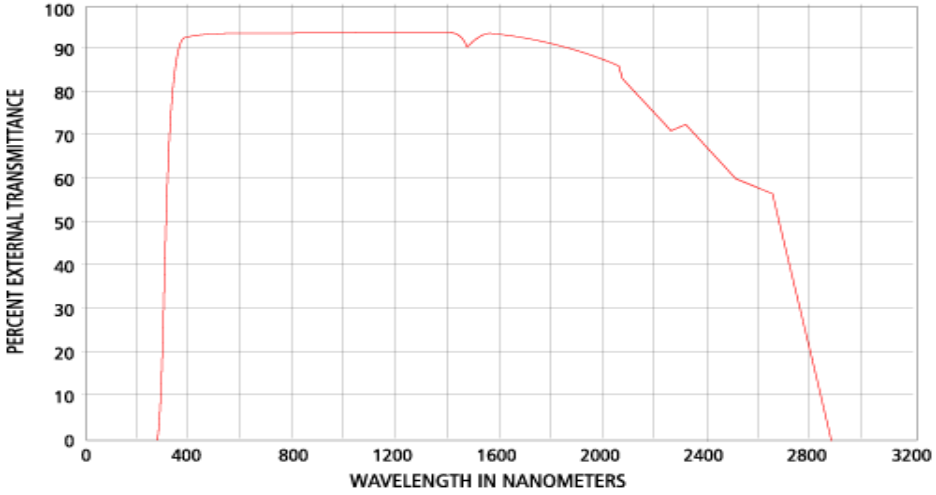

[7] Thorlabs non-polarizing beam splitter #BS013 constructed of two BK7 glass prisms with antireflection coatings on the entrance and exit surfaces. The left plot below shows the transmittance, *T*, of forward beam for the two polarization states through the beamsplitting coating between the prisms. The right plot shows the reflectance, *R*, for a typical broadband antireflection coating. So the total transmittance for the forward light path would be *(1-R)*T*(1-R)*.

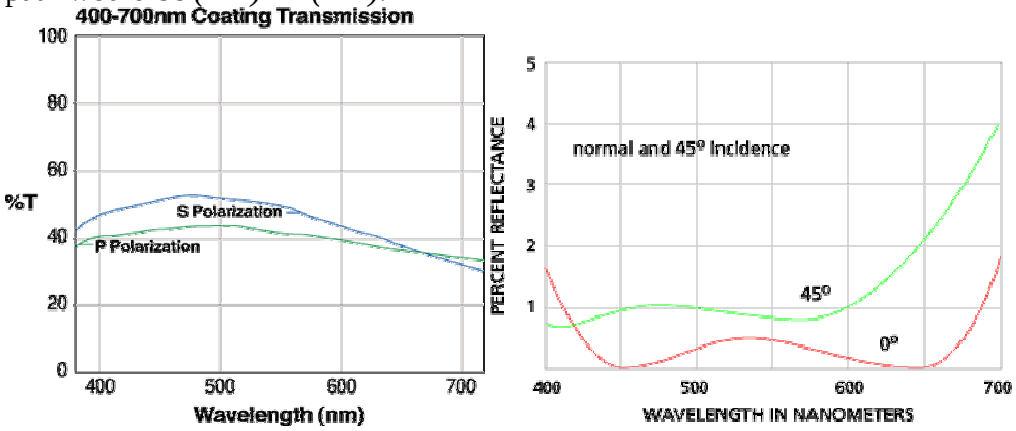

[8] Kodak Neutral Density Attenuators. Kodak publication P-114, 1975. Plot showing the frequency response of a 10% transmittance filter. The transmittance increases significantly above 700 nm. The implications are that the attenuation value must be measured using the AGI setup. At least 3 of the 4 attenuators in the system are of this type.

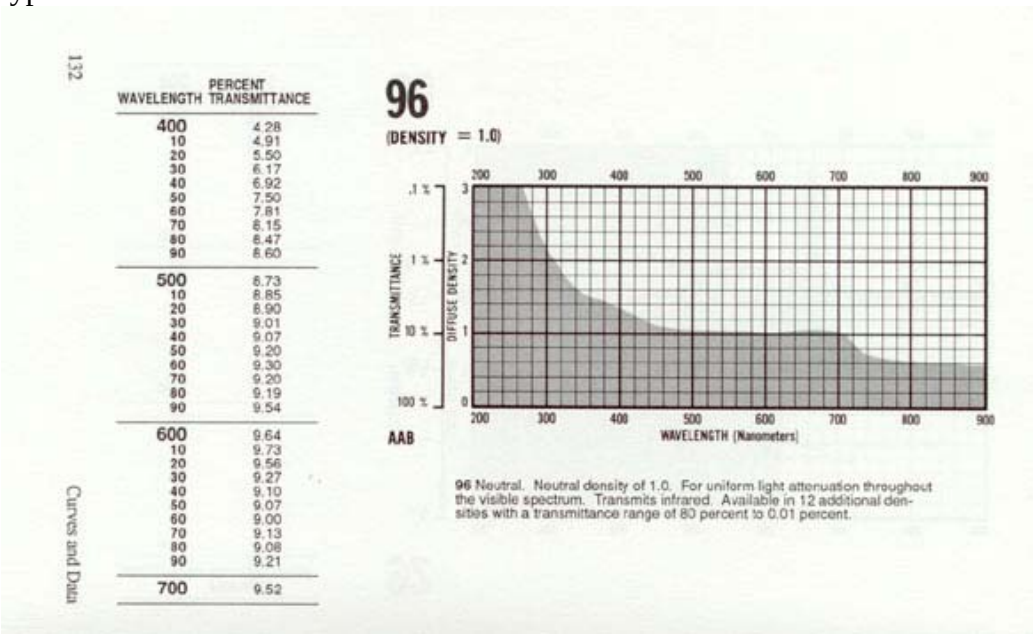

132

WAVELENGTH	PERCENT TRANSMITTANCE
400	4.28
10	4.91
20	5.50
30	6.17
40	6.92
50	7.50
60	7.81
70	8.15
80	8.47
90	8.60
500	8.73
10	8.85
20	8.90
30	9.01
40	9.07
50	9.20
60	9.30
70	9.20
80	9.19
90	9.54
600	9.64
10	9.73
20	9.56
30	9.27
40	9.10
50	9.07
60	9.00
70	9.13
80	9.08
90	9.21
700	9.52

Curves and Data

96

(DENSITY = 1.0)

96 Neutral. Neutral density of 1.0. For uniform light attenuation throughout the visible spectrum. Transmits infrared. Available in 12 additional densities with a transmittance range of 80 percent to 0.01 percent.

[9] A. Hahn, H.W.K. Cheung, *et al.*, **BEAMS-DOC-185-V1**, **BEAMS-DOC-186-V1**, **BEAMS-DOC-587-V3**, **BEAMS-DOC-466-V1**. Background and details of the existing Synchrotron Light system.

[10] R. Coisson, "Angular-spectral distribution and polarization of synchrotron radiation from a 'short' magnet", Phys. Rev. A **20** (1979) 524.

[11] J.D. Jackson, Classical Electrodynamics, John Wiley and Sons, (1962), Ch. 14.

[12] J. Bosser *et al.*, "Proton beam profile measurements with synchrotron light", Nucl. Inst. and Meth. **164** (1979) 375.

[13] E. Lorman, **BEAMS-DOC-1262**, Synclite DAQ reference.

A AGI ACNet Devices

Name	Description
T:AGIBCK	TAGI Perform Background
T:AGIBCT	TAGI Backgnd countdown
T:AGICAL	TAGI Perform Calibration
T:AGICCT	TAGI Calibration count
T:AGIDBG	TAGI Debug Stuff
T:AGIRST	TAGI Remote VME Reset
T:AGISLT	TAGI Perform DAQ
T:AGISTA	TAGI State
	Proton
T:AGPAAO	TAGI Prot pbar AA offset
T:AGPAGA	TAGI Prot AGI Attenuator
T:AGPATT	TAGI Prot Attenuation
T:AGPBK1	TAGI Prot Background AG1
T:AGPBK2	TAGI Prot Background AG2
T:AGPBK3	TAGI Prot Background AG3
T:AGPBSE	TAGI Prot Bkgd Subtract
T:AGPCAB	TAGI Prot Calib Bucket
T:AGPCAD	TAGI Prot cable delay
T:AGPCAV	TAGI Prot Calib. Value
T:AGPDC	TAGI Prot DC Average
T:AGPDCB	TAGI Prot DC Background
T:AGPDCE	TAGI Prot do DC beam
T:AGPDCG	TAGI Prot DC Int Gates
T:AGPDCP	TAGI Prot DC Pedestal
T:AGPDCS	TAGI Prot DC Intensity
T:AGPDCW	TAGI Prot DC Int Width
T:AGPDD	TAGI Prot Dig Pulse Dely
T:AGPDPB	TAGI Prot DC Ped Bckgnd
T:AGPDPS	TAGI Prot DC Ped Intens
T:AGPDW	TAGI Prot Dig Pulse Wdth
T:AGPG1S	TAGI Prot Intensity AG1
T:AGPG2S	TAGI Prot Intensity AG2
T:AGPG3S	TAGI Prot Intensity AG3
T:AGPGI1	TAGI Prot Average AG1
T:AGPGI2	TAGI Prot Average AG2
T:AGPGI3	TAGI Prot Average AG3
T:AGPID1	TAGI Prot Int Delay AG1
T:AGPID2	TAGI Prot Int Delay AG2
T:AGPID3	TAGI Prot Int Delay AG3
T:AGPIPE	TAGI Prot Use Inst Ped
T:AGPIW1	TAGI Prot Int Width AG1
T:AGPIW2	TAGI Prot Int Width AG2

Name	Description
T:AGPIW3	TAGI Prot Int Width AG3
T:AGPOF	TAGI Prot Offset
T:AGPP1S	TAGI Prot Pedestal AG1
T:AGPP2S	TAGI Prot Pedestal AG2
T:AGPP3S	TAGI Prot Pedestal AG3
T:AGPPB1	TAGI Prot Ped Bckgnd AG1
T:AGPPB2	TAGI Prot Ped Bckgnd AG2
T:AGPPB3	TAGI Prot Ped Bckgnd AG3
T:AGPPE1	TAGI Prot Ave Ped AG1
T:AGPPE2	TAGI Prot Ave Ped AG2
T:AGPPE3	TAGI Prot Ave Ped AG3
T:AGPPR1	TAGI Prot Ped RMS AG1
T:AGPPR2	TAGI Prot Ped RMS AG2
T:AGPPR3	TAGI Prot Ped RMS AG3
T:AGPPSE	TAGI Prot Ped Subtract
T:AGPRM1	TAGI Prot RMS AG1
T:AGPRM2	TAGI Prot RMS AG2
T:AGPRM3	TAGI Prot RMS AG3
T:AGPSF	TAGI Prot Scale Factor
T:AGPSLA	TAGI Prot SL Attenuator
T:AGPSAE	TAGI P SL Atten. Enable
T:AGPSAI	TAGI P SL Atten In Lmt
T:AGPSAO	TAGI P SL Atten Out Lmt
T:AGPSQL	TAGI Prot Sum Squelch
T:AGPSUM	TAGI Prot abort gap sum
T:AGPVD1	TAGI Prot HV Delay AG1
T:AGPVD2	TAGI Prot HV Delay AG2
T:AGPVD3	TAGI Prot HV Delay AG3
T:AGPVET	TAGI Prot Veto bunches
T:AGPVEW	TAGI Prot Veto Width
T:AGPVW1	TAGI Prot HV Width AG1
T:AGPVW2	TAGI Prot HV Width AG2
T:AGPVW3	TAGI Prot HV Width AG3
T:AGPHV	TAGI Prot MCP Voltage
	Antiproton
T:AGAAAO	TAGI Pbar prot AA offset
T:AGAAGA	TAGI Pbar AGI Attenuator
T:AGAATT	TAGI Pbar Attenuation
T:AGABK1	TAGI Pbar Background AG1
T:AGABK2	TAGI Pbar Background AG2
T:AGABK3	TAGI Pbar Background AG3
T:AGABSE	TAGI Pbar Bkgd Subtract
T:AGACAB	TAGI Pbar Calib Bucket
T:AGACAD	TAGI Pbar cable delay

Name	Description
T:AGACAV	TAGI Pbar Calib. Value
T:AGADC	TAGI Pbar DC Average
T:AGADCB	TAGI Pbar DC Background
T:AGADCE	TAGI Pbar do DC beam
T:AGADCG	TAGI Pbar DC Int Gates
T:AGADCP	TAGI Pbar DC Pedestal
T:AGADCS	TAGI Pbar DC Intensity
T:AGADCW	TAGI Pbar DC Int Width
T:AGADD	TAGI Pbar Dig Pulse Dely
T:AGADPB	TAGI Pbar DC Ped Bckgnd
T:AGADPS	TAGI Pbar DC Ped Intens
T:AGADW	TAGI Pbar Dig Pulse Wdth
T:AGAG1S	TAGI Pbar Intensity AG1
T:AGAG2S	TAGI Pbar Intensity AG2
T:AGAG3S	TAGI Pbar Intensity AG3
T:AGAGI1	TAGI Pbar Average AG1
T:AGAGI2	TAGI Pbar Average AG2
T:AGAGI3	TAGI Pbar Average AG3
T:AGAID1	TAGI Pbar Int Delay AG1
T:AGAID2	TAGI Pbar Int Delay AG2
T:AGAID3	TAGI Pbar Int Delay AG3
T:AGAIPE	TAGI Pbar Use Inst Ped
T:AGAIW1	TAGI Pbar Int Width AG1
T:AGAIW2	TAGI Pbar Int Width AG2
T:AGAIW3	TAGI Pbar Int Width AG3
T:AGAOF	TAGI Pbar Offset
T:AGAP1S	TAGI Pbar Pedestal AG1
T:AGAP2S	TAGI Pbar Pedestal AG2
T:AGAP3S	TAGI Pbar Pedestal AG3
T:AGAPB1	TAGI Pbar Ped Bckgnd AG1
T:AGAPB2	TAGI Pbar Ped Bckgnd AG2
T:AGAPB3	TAGI Pbar Ped Bckgnd AG3
T:AGAPE1	TAGI Pbar Ave Ped AG1
T:AGAPE2	TAGI Pbar Ave Ped AG2
T:AGAPE3	TAGI Pbar Ave Ped AG3
T:AGAPR1	TAGI Pbar Ped RMS AG1
T:AGAPR2	TAGI Pbar Ped RMS AG2
T:AGAPR3	TAGI Pbar Ped RMS AG3
T:AGAPSE	TAGI Pbar Ped Subtract
T:AGARM1	TAGI Pbar RMS AG1
T:AGARM2	TAGI Pbar RMS AG2
T:AGARM3	TAGI Pbar RMS AG3
T:AGASF	TAGI Pbar Scale Factor
T:AGASLA	TAGI Pbar SL Attenuator

Name	Description
T:AGASQL	TAGI Pbar Sum Squelch
T:AGASUM	TAGI Pbar abort gap sum
T:AGAVD1	TAGI Pbar HV Delay AG1
T:AGAVD2	TAGI Pbar HV Delay AG2
T:AGAVD3	TAGI Pbar HV Delay AG3
T:AGAVET	TAGI Pbar Veto bunches
T:AGAVEW	TAGI Pbar Veto Width
T:AGAVW1	TAGI Pbar HV Width AG1
T:AGAVW2	TAGI Pbar HV Width AG2
T:AGAVW3	TAGI Pbar HV Width AG3
T:AGAHV	TAGI Pbar MCP Voltage

B Original Dynode-gated PMT

The original gated PMT was a dynode-gated type. The gating circuit, which was developed in-house by PPD, holds the dynodes at a potential below the previous dynodes effectively turning off the tube (Figure 14). When the gate is on, the dynodes are pushed up to their nominal operating voltage. Figure 15 shows the schematic for the gating circuit.

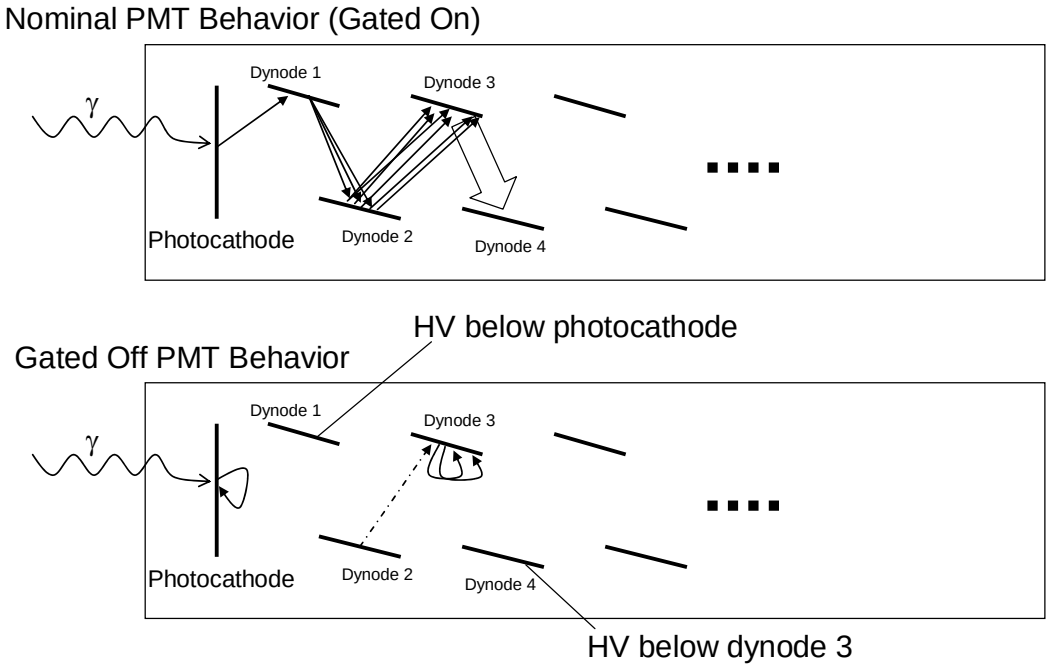

Figure 14: PMT behavior for gated on and gated off modes. the gated on mode looks like an ordinary PMT, while the gated off mode turns around the field lines between several dynodes effectively shutting off the multiplication.

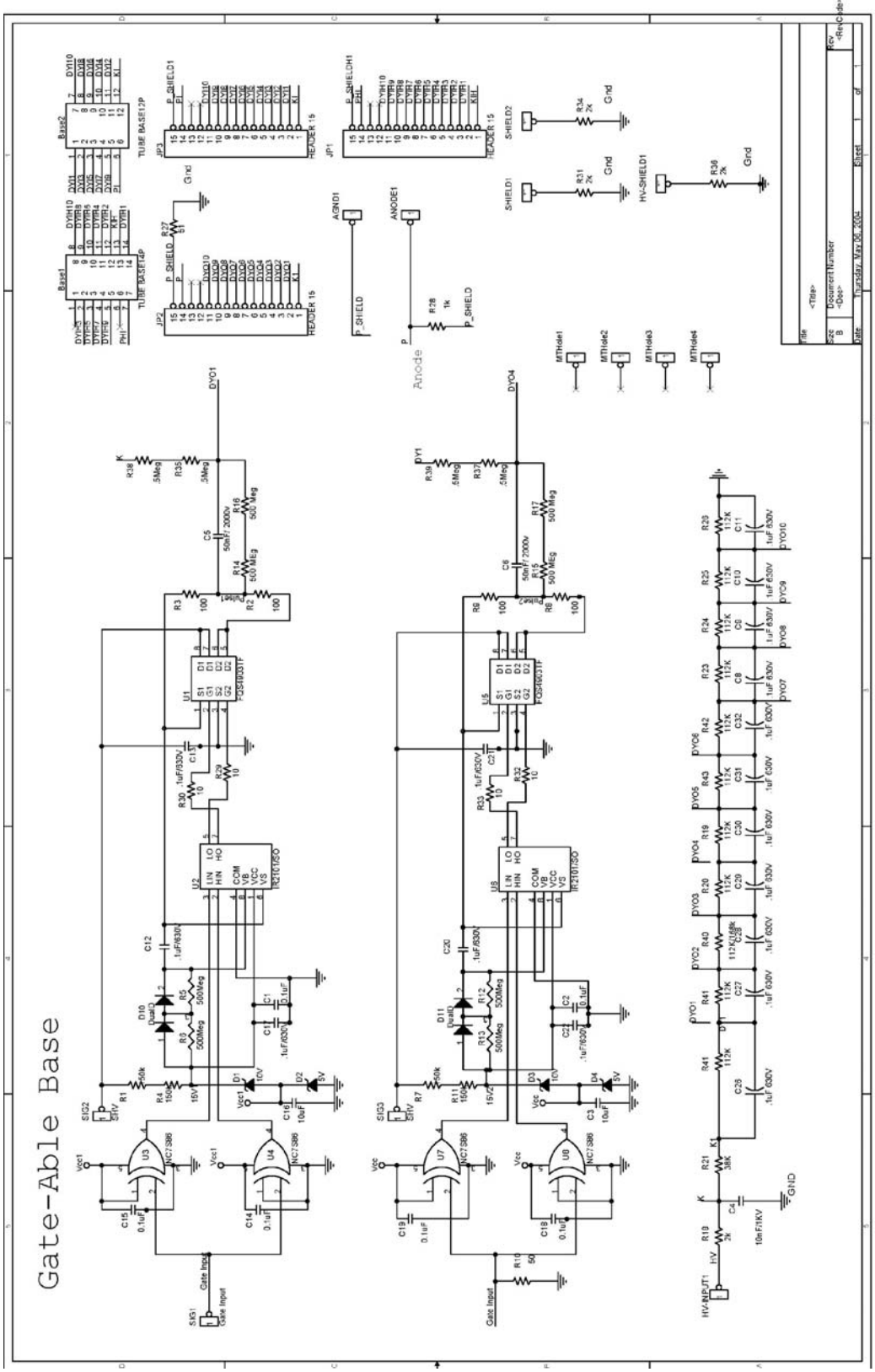

Figure 15: Schematic of the gated base for a 10-stage PMT. A single gate pulse drives 2 FET circuits that are AC coupled into dynodes 1 and 4. The DC state has dynode 1 held ~30V below the photocathode and dynode 4 held at the nominal potential of dynode 1. With interdynode voltages of ~100V, dynode 1 is pulsed with 130V and dynode 4 is pulsed with 300V. These voltages push the dynodes to their nominal values.

Many studies were conducted to determine features of the system such as the extinction ratio, stability of the gain immediately after the gate is applied, and the sensitivity to light present just before the gate is applied. To study these features, a system was set up with two LEDs – a blue pulsed LED to simulate the nominal bunches and a green LED with a tiny DC level to simulate the DC beam.

Three variations of dynode gating were studied: only dynode 2, dynodes 2 and 4, and dynodes 1 and 4. The studies focused mostly on the stability of the gain immediately following application of the gate (Figure 16), and on the sensitivity to light incident on the photocathode immediately before the gate is applied (Figure 17). Tests of the gating combinations demonstrated that gating dynode 1 was essential. Both of the dynode 2 versions exhibited unacceptable sensitivity to pre-gate light. Thus the final choice was to gate dynodes 1 and 4.

Two PMTs were studied: an end window tube (Electron Tubes, 9902B), and a side window tube (RCA or Burle or whoever, 4552). The tests of the PMTs showed that the gain of the side window PMT became stable 200ns into the gate. That time was dominated by post-gate ringing on the anode signal. The end window PMT also had the post-gate ringing, but in addition, had a long transient where the gain slowly increased until it reached a plateau. Both PMTs were resistant to pre-gate light until the light reached 5 or 10 times the typical bunch light intensity. The reason for this sensitivity to light incident before the gate was unknown. At the typical bunch intensities, this sensitivity did not affect the system. Because of the transient in the gain of the end window tube, the 4552 was chosen. Figure 18 shows the flat response of this tube using the dynode 1 and dynode 4 gating circuit.

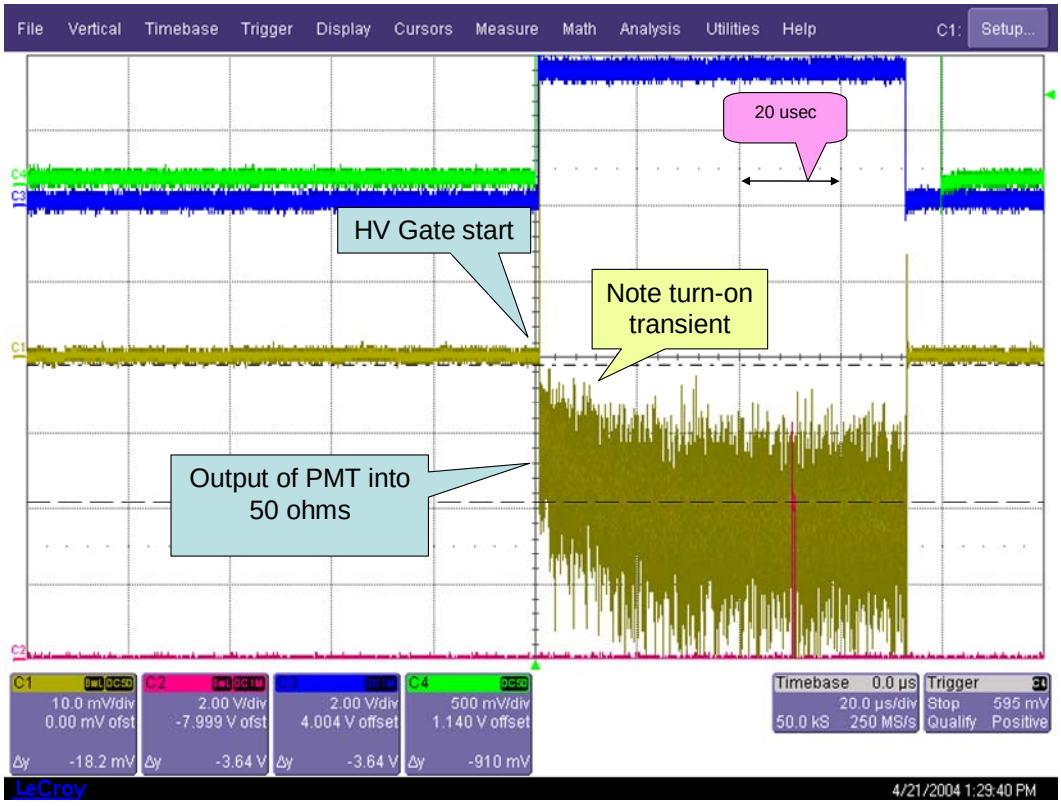

Figure 16: Scope trace showing gain transient at beginning of gate observed in the end window tube. The PMT is observing an LED which is always on. The turn-on transient has a time constant of ~20µs. The source of the transient was thought to be photocathode resistivity but was seemingly ruled out by selectively covering the central part of the photocathode. In any case this tube was not used.

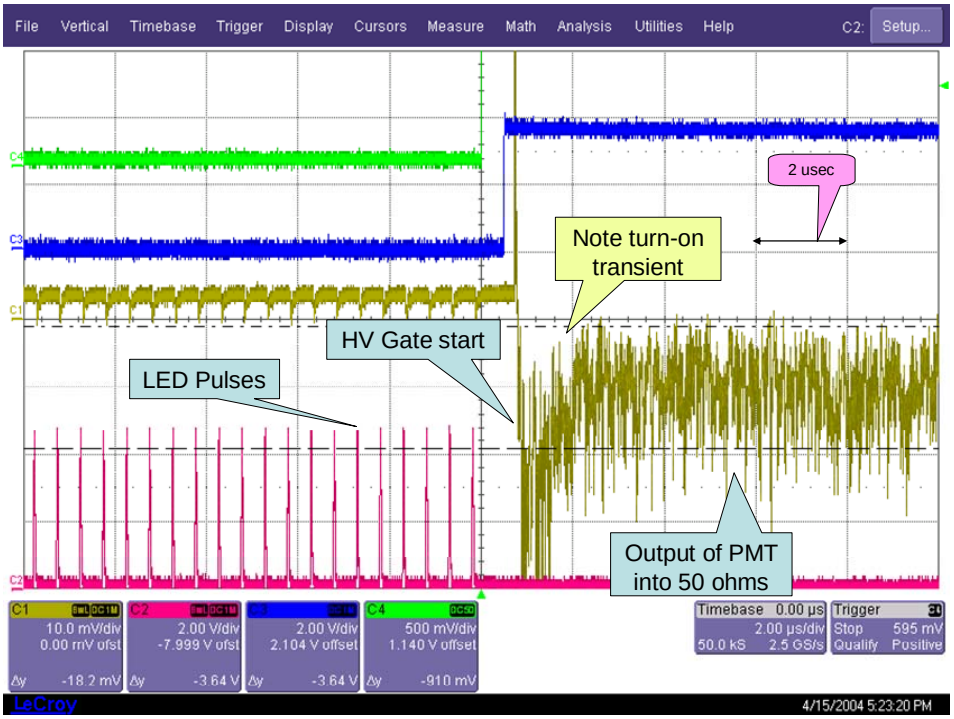

Figure 17: Scope trace demonstrating sensitivity to light present before the gate is applied when gating dynodes 2 and 4. This test uses a pulsed LED to simulate light from bunches. The size of the transient depends on how close the gate is to the last bunch and is not present if the bunch-simulating pulsed LED is not on.

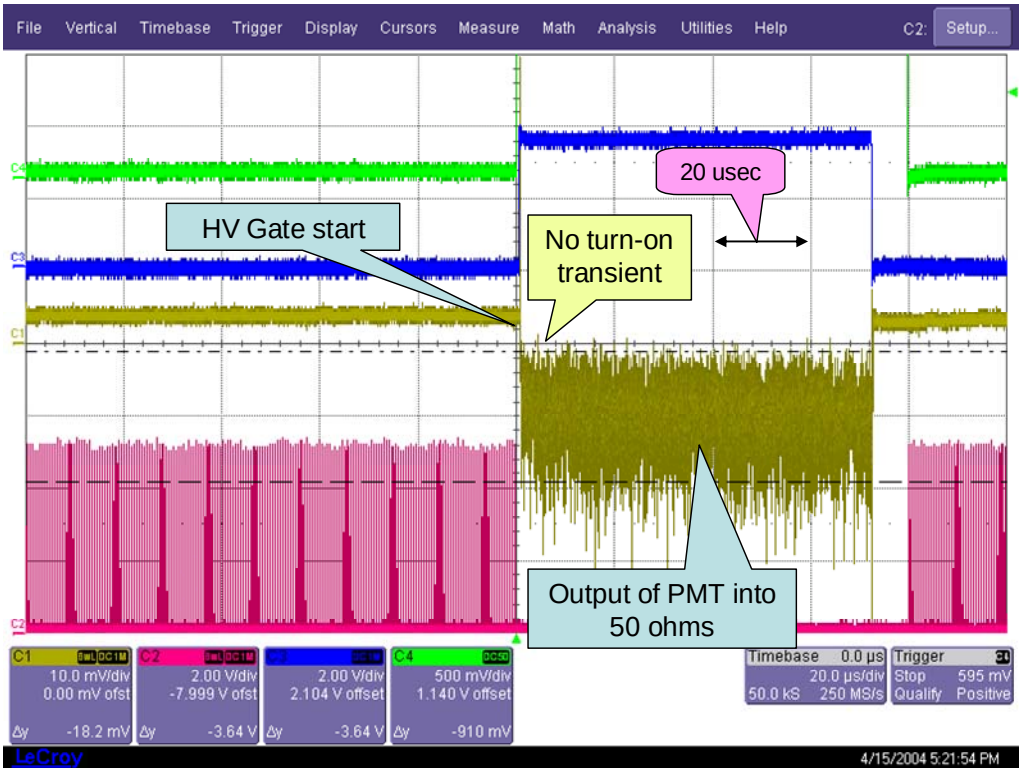

Figure 18: Side window tube with dynode 1 and 4 gated. There is no turn-on transient present in this case. Note that this is the combination that is in use in the abort gap monitor.

C Studies of Hamamatsu MCP-PMT

This is the talk given at a LARP meeting showing results of PMT tests. The last slide shows gains which for that one seemed to indicate a gain of 5 x 10^5. The present PMTs have larger gains.

Bench tests of LBL PMT

- Various pulsers and gate generators provide
  - 12 bunches and a gap (not precise TeV timing)
  - PMT gate
  - Integrator gate
  - Duty cycles (both skipped turns and overall supercycle)
- Fast integrator receives signal and sends to scope
- Scope measures pulse height distribution

Bench Tests of LBL PMT

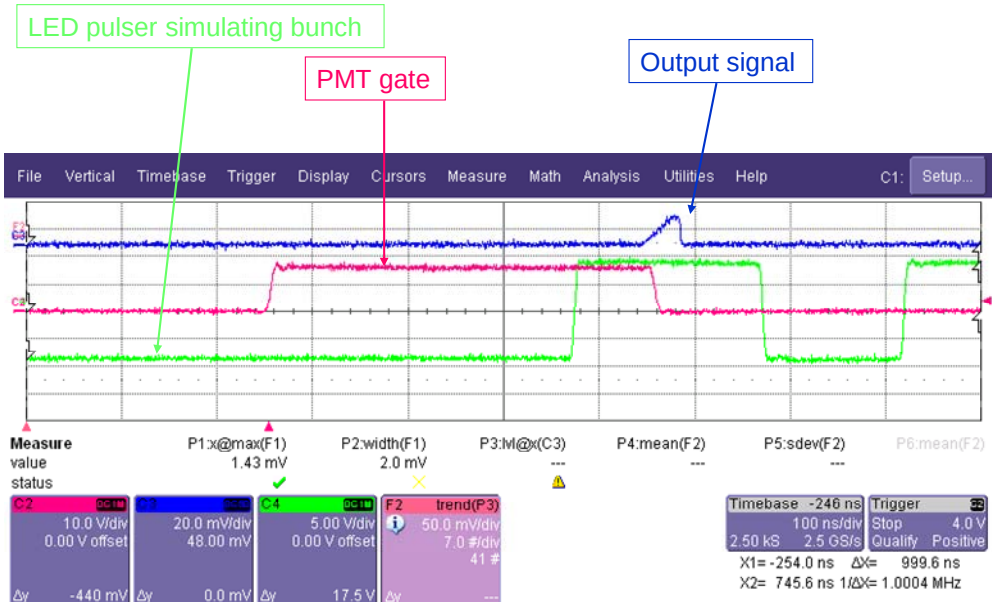

Bench Tests of LBL PMT

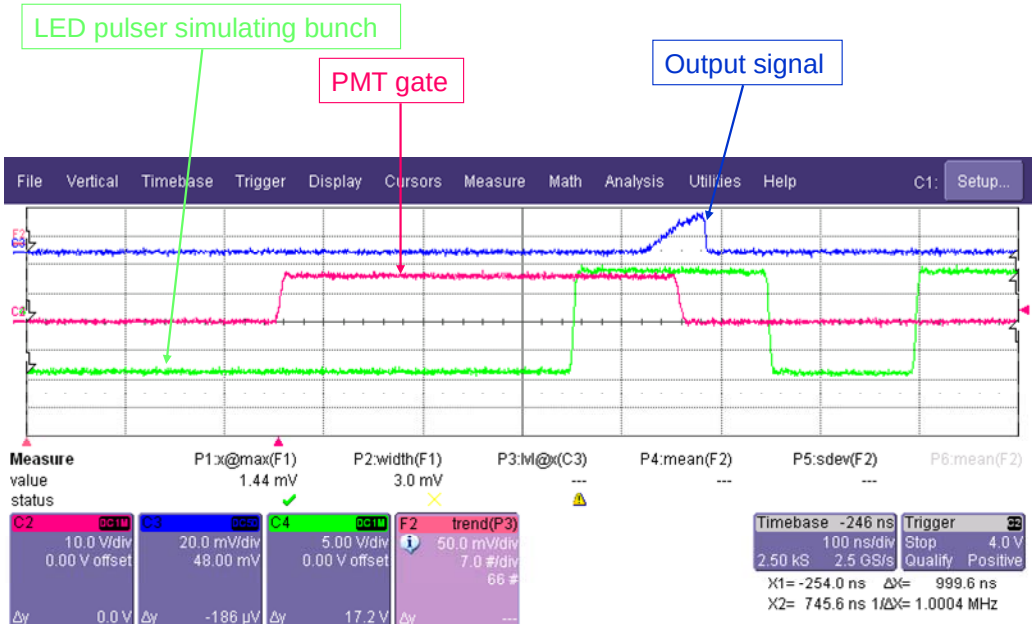

Bench Tests of LBL PMT

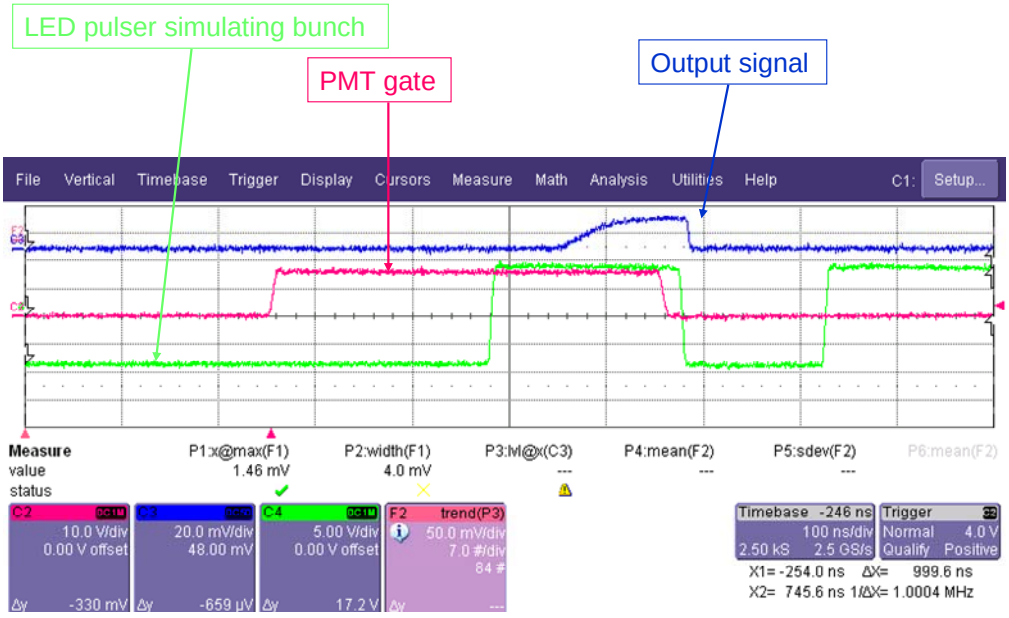

Bench Tests of LBL PMT

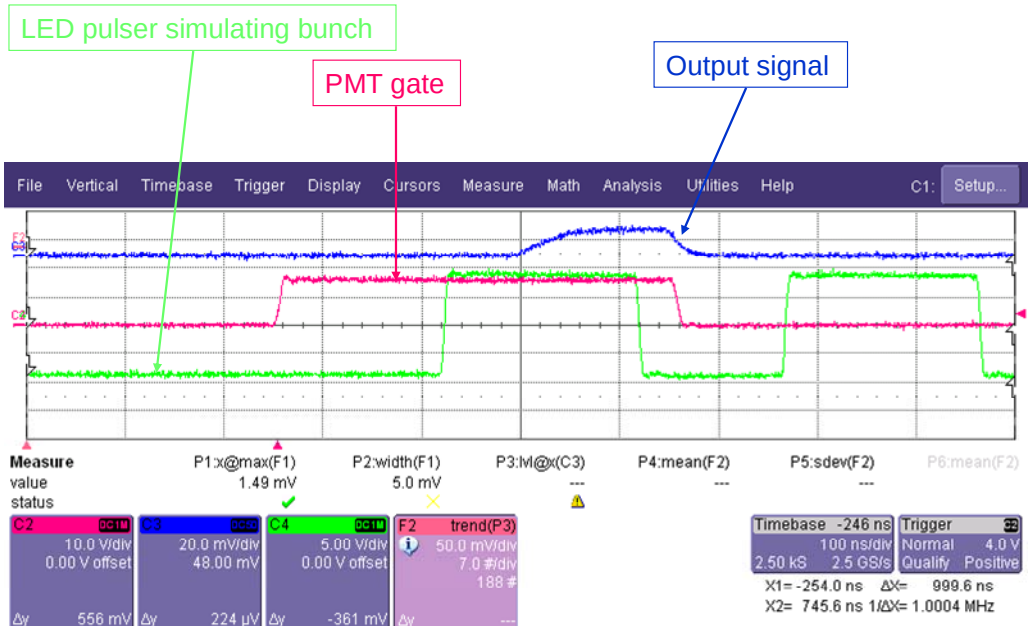

Bench Tests of LBL PMT

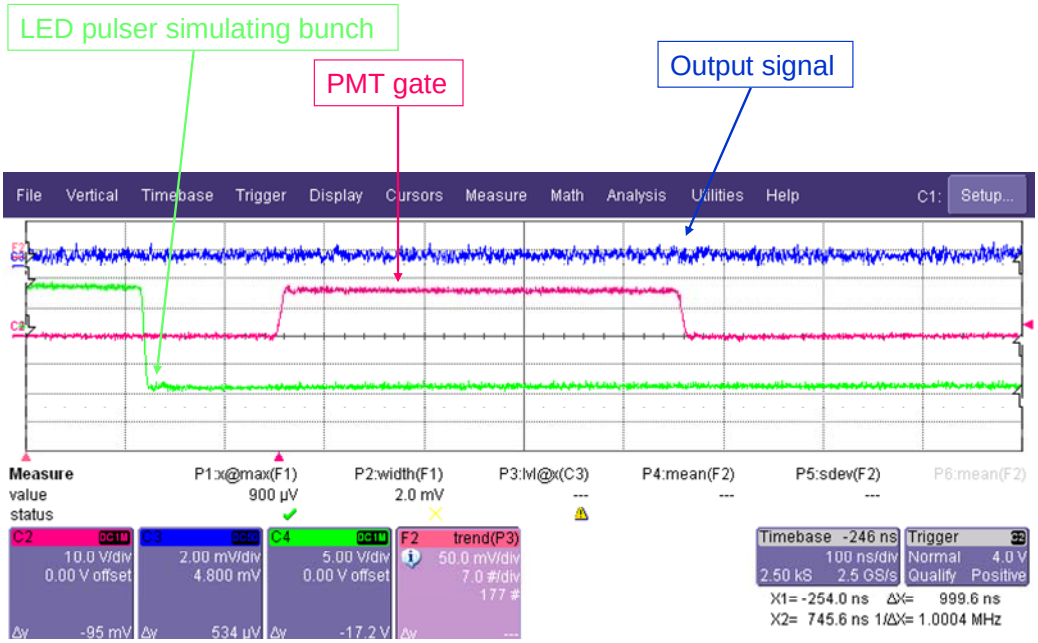

Bench Tests of LBL PMT

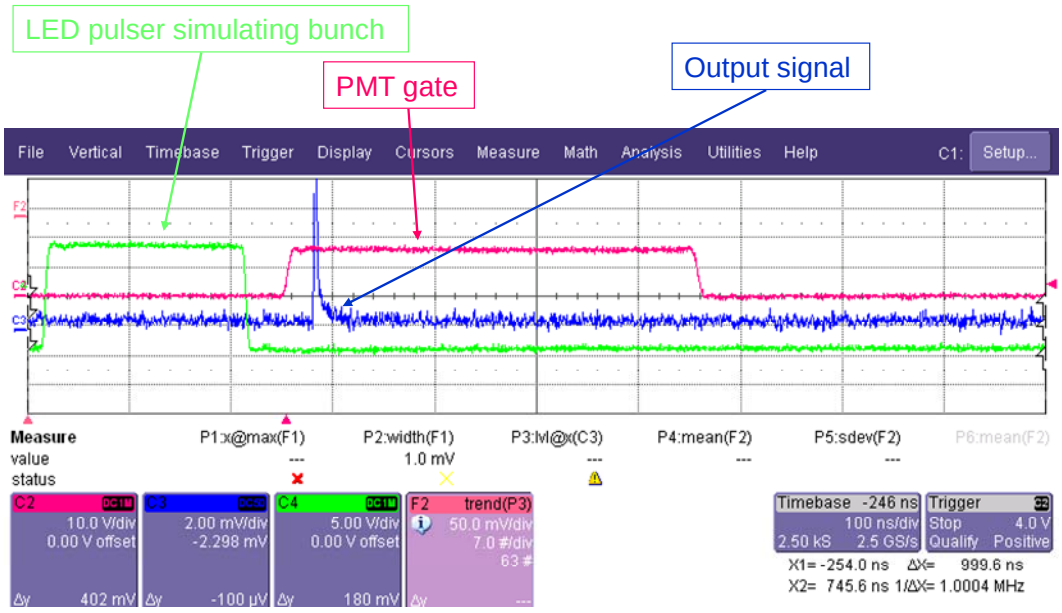

Bench Tests of LBL PMT

Pulse height distributions (w/background)

- Bunch is ~ 1.6 x 10^5 photoelectrons (5 x 10^4 actual)
- AG is ~ 14 photoelectrons / 200ns (~10X > actual)
- Gain of PMT is ~5 x 10^5 at 3347 V (3400 MAX)
  - Expect 10^6 (pulse height / duty cycle problems??)